T Cell Receptor Binding Transition States and Recognition of Peptide/MHC †

Rebecca L. Davis-Harrison,‡ Francis K. Insaidoo,‡ and Brian M. Baker*,‡,§

Department of Chemistry and Biochemistry and Walther Cancer Research Center, 251 Nieuwland Science Hall, University of Notre Dame, Notre Dame, Indiana 46556

Received August 21, 2006; Revised Manuscript Received November 20, 2006

ABSTRACT: T cell receptor recognition of peptide/MHC has been described as proceeding through a "two-step" process in which the TCR first contacts the MHC molecule prior to formation of the binding transition state using the germline-encoded CDR1 and CDR2 loops. The receptor then contacts the peptide using the hypervariable CDR3 loops as the transition state decays to the bound state. The model subdivides TCR binding into peptide-independent and peptide-dependent steps, demarcated at the binding transition state. Investigating the two-step model, here we show that two TCRs that recognize the same peptide/MHC bury very similar amounts of solvent-accessible surface area in their transition states. However, 1300−1500 Å^2 of surface area is buried in each, a significant amount suggestive of participation of peptide and associated CDR3 surface. Consistent with this interpretation, analysis of peptide and TCR variants indicates that stabilizing contacts to the peptide are formed within both transition states. These data are incompatible with the original two-step model, as are transition state models built using the principle of minimal frustration commonly employed in the investigation of protein folding and binding transition states. These findings will be useful in further explorations of the nature of TCR binding transition states, as well as ongoing efforts to understand the mechanisms by which T cell receptors recognize the composite peptide/MHC surface.

T cell receptor (TCR)[1] recognition of a peptide bound and presented by a major histocompatibility complex (MHC) molecule is required for the initiation and propagation of a cellular immune response, as well as selection of the T cell repertoire. Structural studies of TCR-peptide/MHC ternary complexes have indicated that TCRs contact both the peptide and the MHC molecule, with the MHC typically contributing two-thirds or more of the contacted surface area (*1*). Despite the small contribution of the peptide to the buried surface, TCRs generally maintain high levels of peptide specificity, but this is contrasted by an inherent cross-reactivity (reviewed in refs *2* and *3*). This duality of specificity and cross-reactivity is a key feature of T cell biology, yet a clear picture of its physical basis has yet to emerge. Although recent descriptions of cross-reactive binding suggest that it remains highly peptide-specific (*3*, *4*), degenerate peptide/MHC binding has been implicated in a variety of T cell functions, including thymic selection (*5*), the scanning of multiple peptides (*6*), and TCR signaling (*7*).

On the basis of Φ analysis (*8*), or the effects of mutations on association kinetics relative to their effects on binding affinities, Wu et al. have proposed a conceptually appealing yet controversial two-step model for TCR recognition of peptide/MHC (*9*). This model, which neatly integrates the concepts of peptide specificity and binding degeneracy, posits that the germline-encoded TCR CDR1 and/or CDR2 loops are driven to contact the MHC molecule early in the recognition process, prior to the occurrence of the TCR-peptide/MHC binding transition state. Contacts to the peptide are then made as the transition state decays to the bound state. The model subdivides the ligand recognition process into peptide-independent and peptide-dependent steps, demarcated at the binding transition state.

Other than the Φ analysis of Wu et al. (*9*), there have been few characterizations of TCR-peptide/MHC transition states that could yield insight into this process. A number of studies have measured activation energies for TCR binding (*6*, *10*−*12*), indicating that movement of a TCR from the unbound state to the transition state is typically characterized by a high activation enthalpy and either a positive or negative activation entropy. However, as these thermodynamic values are also dependent upon the properties of the unligated proteins, they cannot be directly used to infer structural details about the association phase of the binding reaction. An exception is the elegant study of Lee et al. (*12*), who showed that the G10 TCR recognizes a native and single amino acid variant HIV epitope bound to the class I MHC HLA-A2 with nearly identical activation thermodynamics, despite the observation that the two peptides have different conformations in the free peptide/MHC complexes. Assuming that the conformation of the peptides is similar in the

† Supported by Grant GM067079 from the National Institute of General Medical Sciences, National Institutes of Health.

* Corresponding author. E-mail: bbaker2@nd.edu. Phone: (574) 631-9810. Fax: (574) 631-6652.

‡ Department of Chemistry and Biochemistry, University of Notre Dame.

§ Walther Cancer Research Center, University of Notre Dame.

[1] Abbreviations: TCR, T cell receptor; MHC, major histocompatibility complex; CDR, complementarity determining region; RMSD, root mean square deviation; MD, molecular dynamics.

10.1021/bi061702p CCC: $37.00
Published on Web 01/24/2007

TCR-bound states, these results suggest that peptide conformational changes occur upon relaxation from the transition state to the bound state, i.e., after formation of the TCR-peptide/MHC transition state.

A6 and B7 are two different TCRs that both recognize the Tax peptide (LLFGYPVYV) presented by HLA-A2. The A6 and B7 TCRs bind Tax/HLA-A2 with nearly identical affinities and kinetics, and they both bury approximately 2000 Å^2 of solvent-accessible surface area in the bound state (*10*, *13*, *14*). We recently showed that the thermodynamics associated with movement from the unbound states to the transition states are also very similar for A6 and B7, although there are large differences in the thermodynamics for movement from the transition states to the bound states (*10*). The similarities in the association phases of the A6 and B7 binding reactions are consistent with a common association mechanism as predicted by the two-step binding model, although, as noted above, the thermodynamic values provide no details regarding the structural properties of the transition states.

To gain further insight into the nature of the A6 and B7 binding transition states (or, more formally, the transition state ensembles), we used *m* values, or the dependence of free energies on denaturant, to measure the amount of solvent-accessible surface area buried in the two binding transition states. Again consistent with the two-step model, we find that the A6 and B7 transition states are very similar: both transition states bury 65−70% of the total buried surface area, amounting to 1300−1500 Å^2. However, burial of such a large amount of surface in either transition state is unlikely to be achieved by the germline-encoded CDR1 and CDR2 loops alone, suggesting large contributions from the CDR3 loops and the Tax peptide. Consistent with this interpretation, analysis of peptide and TCR variants via Φ analysis indicates that stabilizing contacts to the central tyrosine of the Tax peptide are formed within both transition states. The data are thus in conflict with the two-step model as originally formulated, as are transition state models generated using the principle of minimal frustration (i.e., binding reactions proceeding with a low probability for contacts in the transition state that are not present in the bound state) (*15*−*17*). These results are discussed in terms of both specific A6 and B7 recognition of Tax/HLA-A2 and TCR recognition of peptide/MHC in general and will be useful in further explorations of the nature of TCR binding transition states and ongoing efforts to understand the mechanisms by which T cell receptors recognize the composite peptide/MHC surface.

MATERIALS AND METHODS

Proteins and Peptides. Wild-type and mutant A6 and B7 TCRs and peptide/HLA-A2 complexes were refolded from *Escherichia coli* inclusion bodies and purified as described (*10*). Peptide/HLA-A2 concentrations were determined spectrophotometrically as described (*10*). Peptides were synthesized and purified locally using an ABI 433A instrument. Peptide purity and molecular weight were confirmed by analytical HPLC/mass spectrometry. The S31αA and Y104βA mutants of the A6 and B7 TCRs were generated via QuickChange mutagenesis (Strategene) and refolded and purified similarly to wild type. Mutations were confirmed via forward and reverse DNA sequencing.

Biacore Measurements. Steady-state and kinetic Biacore experiments were performed as described (*10*). Briefly, A6 or B7 TCR was coupled to a CM5 sensor chip using amine coupling. Peptide/MHC was injected over both reference and ligand-coupled cells simultaneously, and each injection was repeated twice. For steady-state experiments, a flow rate of 5 μL/min was used. Two separate concentration series were injected, from 1 to 50 μM. For kinetic experiments, the flow rate was 100 μL/min. Two separate concentration series were injected, ranging from 3 to 100 μM depending on the experiment. All injections were double-referenced using buffer injections and protein injections over a blank flow cell (*18*). Experiments were performed at 25 °C in HBS-EP buffer (10 mM HEPES, 150 mM NaCl, 3 mM EDTA, 0.005% surfactant P20, pH 7.4) prepared in our laboratory with the indicated concentration of urea. HBS-EP/urea solutions were made fresh the day of each experiment. In the urea experiments, to minimize any influence of weaker peptide binding to HLA-A2, we avoided the use of low Tax/HLA-A2 concentrations and maintained the Biacore sample block at 4 °C.

Analysis of Binding and Dissociation Data. Binding and dissociation data as a function of urea concentration were analyzed globally to provide free energy changes in the absence of urea and the derivatives of ΔG with respect to urea concentration, or *m* values. For the steady-state binding data, 22 (A6) or 24 (B7) data sets were fit globally to a single-site binding model of the form:

$$\mathrm{RU} = \mathrm{RU}_{\max}\frac{K'[\text{Tax/HLA-A2}]}{1 + K'[\text{Tax/HLA-A2}]} \tag{1}$$

where K' was represented as

$$K' = \exp\left(-\frac{\Delta G^\circ + m^\circ_{\mathrm{eq}}[\text{urea}]}{RT}\right) \tag{2}$$

$\mathrm{RU}_{\max}$ in eq 1 was a local variable for each data set indicating the activity of each surface, whereas ΔG° and m°_{eq} in eq 2 were global variables common to all data sets. ΔG° thus represents the binding free energy change in the absence of urea, and m°_{eq} represents $\partial\Delta G^\circ/\partial$[urea]. For presentation of the steady-state binding data in Figure 1, each data set was normalized to its fitted $\mathrm{RU}_{\max}$ to illustrate the effects of urea on binding.

For dissociation data, 55 (A6) or 44 (B7) Biacore dissociation phases were normalized to the beginning value and globally fit to a single-exponential decay of the form:

$$y = A_0 \exp(-k't) + b \tag{3}$$

where k' was represented as

$$k' = \left(\frac{k_b T}{h}\right)\exp\left(-\frac{\Delta G^{\ddagger}_{\mathrm{off}} + m^{\ddagger}_{\mathrm{off}}[\text{urea}]}{RT}\right) \tag{4}$$

A_0 and b in eq 3 were local variables for each data set indicating initial amplitudes and baseline offsets, whereas $\Delta G^{\ddagger}_{\mathrm{off}}$ and $m^{\ddagger}_{\mathrm{off}}$ in eq 4 were global variables common to all data. $\Delta G^{\ddagger}_{\mathrm{off}}$ represents the activation free energy for dissociation in the absence of urea, and $m^{\ddagger}_{\mathrm{off}}$ represents $\partial\Delta G^{\ddagger}_{\mathrm{off}}/\partial$[urea]. Approximately 2 s of data was excluded from the beginning of the Biacore dissociation phases to

account for disturbances arising from subtraction of the bulk refractive index shift. The differing number of data sets for A6 vs B7 was due to the improved activity of A6 on Biacore CM5 sensor surfaces (*10*). No statistically significant changes were seen in the fitted global parameters if the number of A6 dissociation phases fitted was reduced to the same number of B7 dissociation phases, owing to the large number of degrees of freedom in the global analyses (see below).

Global analysis was performed with OriginPro 7.5 (OriginLab). The steady-state analyses had 257 degrees of freedom for the measurements with A6 and 219 for the measurements with B7. The dissociation analyses had 13091 degrees of freedom for A6 and 9775 for B7. There was no significant parameter correlation in any of the four analyses. Values of R^2 for each fit were >0.99.

The value of $m^{\ddagger}_{on}$, or the dependence of the activation free energy for association on urea concentration, was calculated from the sum of m°_{eq} and $m^{\ddagger}_{off}$. We used this approach rather than fitting Biacore on-rates as a function of urea, as off-rates are more objectively determined by surface plasmon resonance and more easily lend themselves to the kind of global analyses performed here. Furthermore, the concentrations used in the kinetic experiments were not optimal for determining accurate on-rates across all urea concentrations (*18*).

Errors in *m* values were propagated to account for the error in $m^{\ddagger}_{on}$ and the $m^{\ddagger}_{on}/m^{\circ}_{eq}$ ratio. Φ values were determined using $-\ln(k_{on,mutant}/k_{on,wild\ type})/\ln(K_{D,mutant}/K_{D,wild\ type})$, accounting for and propagating experimental error in rates and equilibrium constants to arrive at experimental errors in Φ. When both were available, calculations of Φ values used affinities determined by steady-state rather than kinetic measurements. Error propagation was performed using standard statistical approaches as described (*10*). All errors and error bars are reported at one standard deviation.

Binding data for the TCR mutants and Tax-Y5W peptide were analyzed similarly, except that experiments were not collected as a function of urea. Affinities were determined by analysis of steady-state binding data, off-rates by analysis of Biacore dissociation rates, and on-rates from the ratio of k_{off} to K_D.

CD Spectroscopy. CD spectra as a function of urea were collected at 25 °C using an Aviv 62DS instrument. Protein solutions of 3 μM were prepared in 20 mM NaH_2PO_4 and 75 mM NaCl, pH 7.4. Urea was added to 0.2, 0.4, 0.6, 0.8, and 1 M concentrations using a stock concentration of 6.25 M urea, 20 mM NaH_2PO_4, and 75 mM NaCl, pH 7.4.

Peptide Dissociation. Peptide dissociation from HLA-A2 in 0.6 M urea was measured using steady-state fluorescence anisotropy with a fluorescent Tax peptide variant (Tax-3K5Flc) as described (*19*). Briefly, 7.5 nM labeled peptide/HLA-A2 was mixed with 7.5 μM unlabeled Tax peptide and the decrease in anisotropy measured vs time using a Beacon 2000 instrument (Invitrogen). Conditions were 10 mM HEPES, 150 mM NaCl, and 0.6 M urea, pH 7.4, at 25 °C. Data were fit using a single-exponential decay function.

Molecular Dynamics Simulations. Coordinates for the free TCRs were extracted from the A6- and B7-Tax/HLA-A2 crystal structures (*13, 14*). Missing side chains were added using the WHATIF server (*20*). For the A6 TCR, the Cα domain was modeled in using the coordinates from the A6-Tax-P6A/HLA-A2 crystal structure (*21*). Hydrogens were added using the Protonate tool of the AMBER 8 suite (*22*). Using the xLEaP tool, the TCRs were immersed in TIP3P water boxes such that no protein atoms were less than 12 Å from any side. Sodium cations were added for neutrality. This resulted in systems consisting of 61914 atoms for the A6 TCR and 62749 atoms for the B7 TCR. Dynamics simulations were then performed using the Sander module, with parameters from the parm99 set. Equilibration consisted of 10000 steps of conjugate gradient energy minimization, followed by 20 ps of MD with restraints applied to the proteins to equilibrate the water. A series of energy minimizations were then carried out to relax the proteins, whereby the restraints were gradually eliminated. The systems were then warmed to 300 K over three MD simulations for a total of 480 ps of dynamics. This was followed by production runs of 16.9 ns for A6 and 16.4 ns for B7. The SHAKE algorithm was used, allowing the use of a 2 fs time step. Long-range electrostatics were treated via particle mesh Ewald. Trajectory analysis was carried out with the Ptraj tool.

Determination of Buried Surface Areas. Buried solvent-accessible surface areas were calculated with the program ACCESS (Scott Presnell), using a probe radius of 1.4 Å and a slice width of 0.05 Å. Buried surface areas were determined as the negative of the surface area of the complex minus the sum of the surface areas of the two free proteins. Coordinates of the free A6 and B7 TCRs either were extracted from the A6- or B7-Tax/HLA-A2 crystal structures or were from molecular dynamics simulations of the free receptors. For determination of surface areas buried by individual CDR loops or loop combinations, calculations were done using only the coordinates for the CDR loop amino acids for the TCR components.

RESULTS

Equilibrium and Kinetic m Values for the Interactions of A6 and B7 with Tax/HLA-A2 Indicate Their Transition States Bury Similar Amounts of Surface Area. Commonly reported in protein denaturation experiments, an *m* value is the dependence of the free energy change on the concentration of denaturant, typically urea or guanidine hydrochloride (recently reviewed in ref *23*). As chemical denaturants destabilize proteins by preferentially interacting with the protein rather than solvent (*24*, *25*), *m* values are also a representation of a protein's solvent-accessible surface area (*26*). *m* values can be determined for equilibrium measurements, i.e., the dependence of the unfolding free energy change on denaturant (m°_{eq}), as well as for kinetic measurements, i.e., the dependence of the folding or unfolding rate on denaturant ($m^{\ddagger}$). The ratio of kinetic-to-equilibrium *m* values ($m^{\ddagger}/m^{\circ}_{eq}$) has seen considerable use in the field of protein folding (e.g., refs *27*−*31*), as this ratio provides the amount of surface area buried in the transition state relative to the amount of surface area buried in the folded state. This ratio is often interpreted as a measure of the amount of "native-like" character possessed by a folding transition state.

Ratios of *m* values can also be used to study protein−protein interactions, reporting on the amount of surface area buried in the binding transition state relative to the fully bound state. Although only a small number of studies have

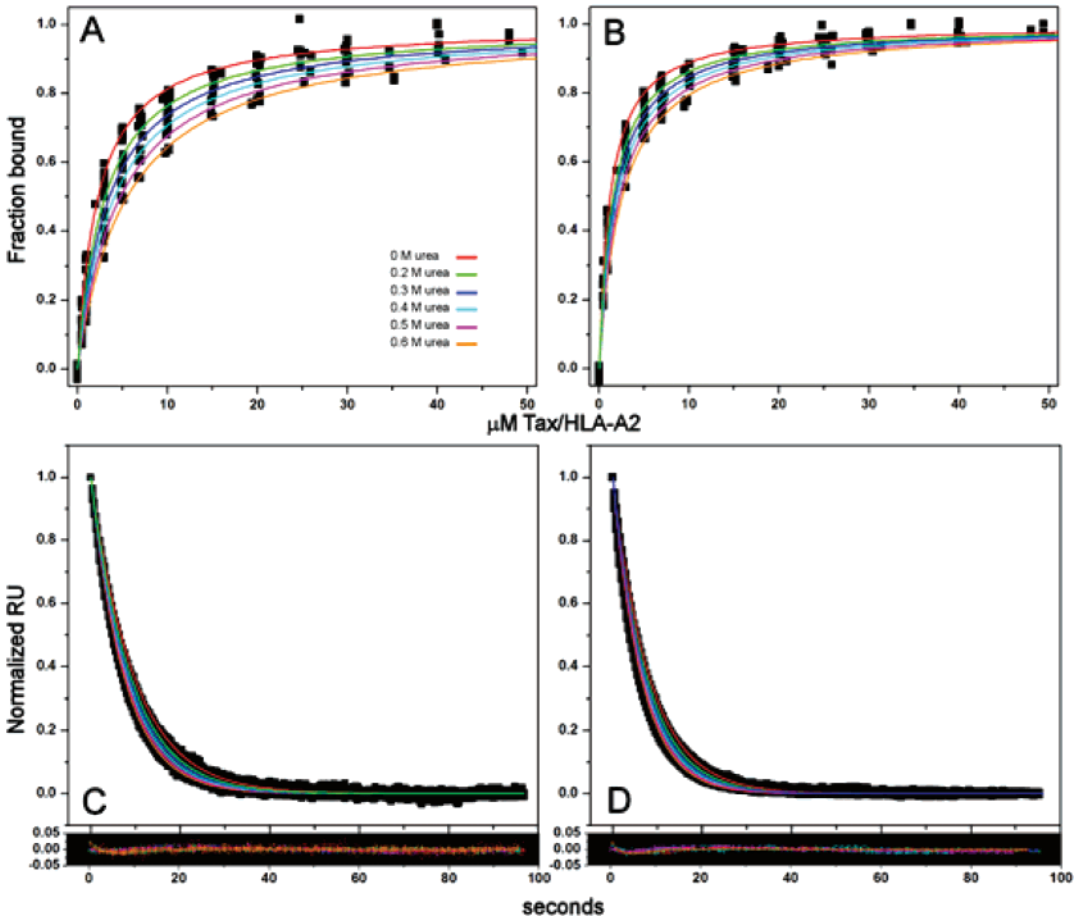

FIGURE 1: Surface plasmon resonance data for A6 and B7 binding Tax/HLA-A2 as a function of urea concentration. (A, B) Steady-state equilibrium data for the A6 (A) and B7 (B) interactions. (C, D) Biacore dissociation phases for the A6 (C) and B7 (D) interactions. Residuals for the dissociation phases are below the plots. Steady-state and kinetic data were globally fit as described in Materials and Methods. For all panels red lines indicate responses at 0 M urea, green, 0.2 M urea, blue, 0.3 M urea, cyan, 0.4 M urea, purple, 0.5 M urea, and yellow, 0.6 M urea. Lines were generated from use of the fitted parameters in eqs 1−4. The residuals for the kinetic data represent the differences between each data set, and lines were calculated using the global and local parameters from the global fit.

been performed (*32*−*34*), the available data indicate that protein−protein interactions can bury between 50% and 80% of their total buried surface within the binding transition state.

To examine the transition states formed between the A6 and B7 TCRs and Tax/HLA-A2, we measured TCR binding affinities and dissociation kinetics as a function of urea concentration, with urea ranging from 0 to 0.6 M. Higher urea concentrations were avoided in order to limit destabilization of the proteins. Measurements were performed using surface plasmon resonance with the A6 or B7 TCRs coupled to the sensor surfaces. Experiments were performed under conditions to maximize SPR data quality (*18*); our previous work demonstrated no dependence of binding parameters on coupling method or which protein was tethered to the surface (*10*, *21*, *35*). Steady-state binding and kinetic dissociation data were analyzed globally as described in Materials and Methods to determine the equilibrium and kinetic *m* values. Data are shown in Figure 1. As expected, the affinities weakened and dissociation rates increased with increasing urea. Figure 2 shows the data in traditional linear form, with free energies determined from individual fits to the data at each concentration of urea and straight lines generated from the results of the four global analyses.

The global parameters from each fit are shown in Table 1. The free energy changes in the absence of urea compare very well with those determined previously for the interactions of A6 and B7 with Tax/HLA-A2: our analysis yielded values for K_D and k_{off} of 2.3 μM and 0.10 s^{-1} for A6 and 1.3 μM and 0.12 s^{-1} for B7; we previously reported values of 2.2 μM and 0.11 s^{-1} for A6 and 1.4 μM and 0.13 s^{-1} for B7 (*10*). The various *m* values for A6 and B7 are slightly different, consistent with the differing composition of the two protein−protein interfaces (*10*). There is a good correlation of the on, off, and equilibrium *m* values for each interaction with the various heat capacity changes determined previously (*10*), as expected from the relationship of both parameters to changes in solvation (*26*) (R^2 values for heat capacity vs *m* value plots are 0.99 for both the A6 and B7 data alone and 0.91 for both data sets combined; if the association values, which were derived from the equilibrium and dissociation values, are excluded, the correlation is 0.93). Most interestingly, the kinetic-to-equilibrium *m* value ratios are very similar for the A6 and B7 interactions and indicate that the receptors bury 65−70% of the total buried solvent-accessible surface area within their transition state ensembles.

Low Urea Concentrations Have Little Influence on Protein Structure or Activity. To examine the effects of urea on the A6 and B7 T cell receptors and the Tax/HLA-A2 complex, we collected CD wavelength spectra as a function of urea concentration (Figure 3). Due to poor signal to noise at high urea concentrations and possibly irreversible unfolding transitions, we could not collect a complete protein dena-

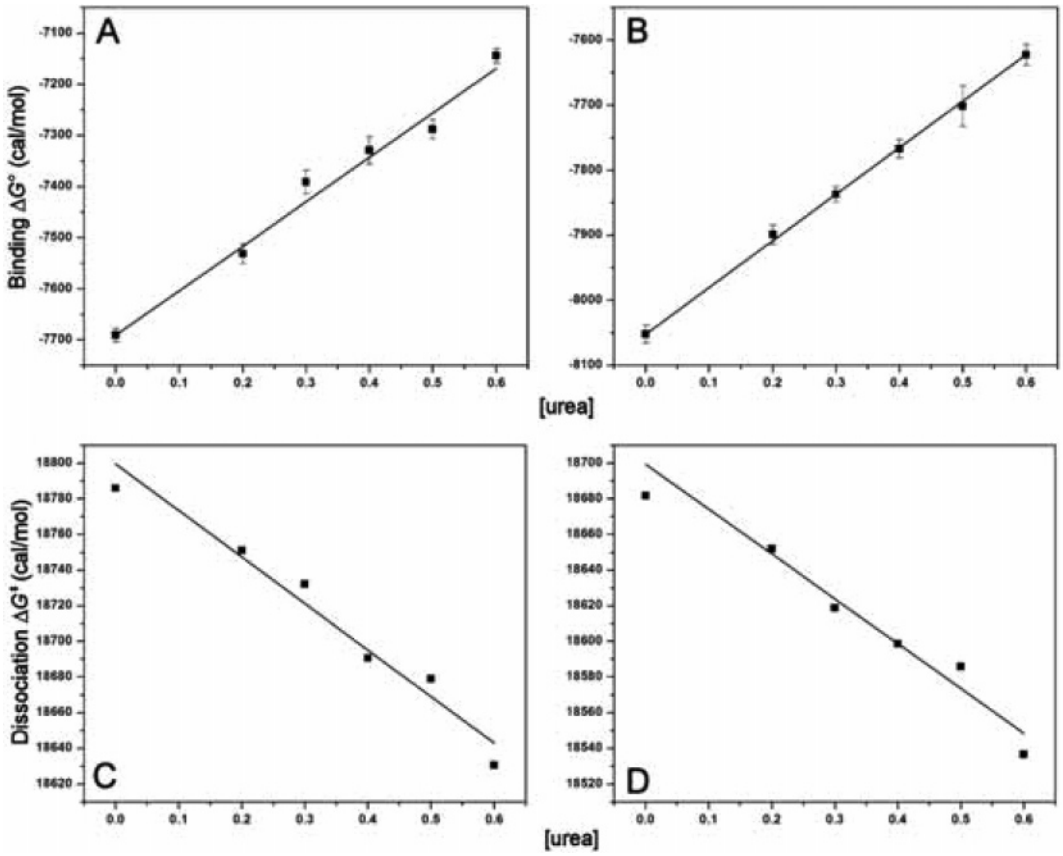

FIGURE 2: TCR binding free energies and activation energies for dissociation as a function of urea concentration. (A, B) Binding free energies for A6 (A) and B7 (B). (C, D) Activation free energies for dissociation of A6 (C) and B7 (D) from Tax/HLA-A2. For all panels, points were generated from individual fits to the data at the indicated concentration of urea and lines from the global parameters shown in Table 2.

Table 1: Global Parameters for Analysis of A6 and B7 Binding Tax/HLA-A2 as a Function of Urea Concentration

TCR	$\Delta G°$ [a]	K_D [b]	m_{eq}° [c]	$\Delta G_{off}^{\ddagger}$ [d]	k_{off} [e]	$m_{off}^{\ddagger}$ [f]	$m_{on}^{\ddagger}$ [g]	$m_{on}^{\ddagger}/m_{eq}^{\circ}$ [h]
A6	-7691.0 ± 11.7	2.3	868.7 ± 38.3	18799.6 ± 0.5	0.10	-261.0 ± 1.4	607.7 ± 38.3	0.70 ± 0.05
B7	-8050.7 ± 8.2	1.3	716.2 ± 40.5	18699.4 ± 0.6	0.12	-251.4 ± 1.7	464.8 ± 40.5	0.65 ± 0.07

[a] Binding free energy in 0 M urea determined from global analysis of steady-state binding data as a function of urea; units of cal/mol. [b] Binding affinity calculated from binding $\Delta G°$. [c] Dependence of $\Delta G°$ on urea determined from global analysis of steady-state binding data as a function of urea; units of cal mol^{-1} M^{-1}. [d] Activation free energy for dissociation in 0 M urea determined from analysis of dissociation kinetics as a function of urea; units of cal/mol. [e] Dissociation rate in units of s^{-1} calculated from $\Delta G_{off}^{\ddagger}$. [f] Dependence of $\Delta G_{off}^{\ddagger}$ on urea determined from global analysis of dissociation kinetics as a function of urea; units of cal mol^{-1} M^{-1}. [g] Dependence of $\Delta G_{on}^{\ddagger}$ on urea calculated from m_{eq}° and $m_{on}^{\ddagger}$. [h] Surface area buried in the binding transition state relative to surface area buried in the fully bound state.

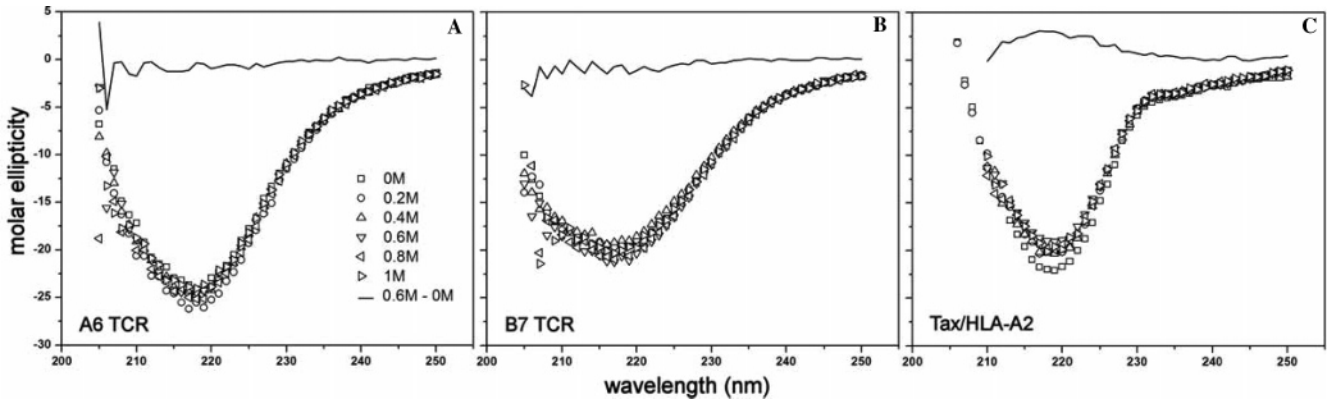

FIGURE 3: CD spectra of A6, B7, and Tax/HLA-A2 as a function of urea concentration. Concentrations of urea, from 0 to 1 M, are indicated. Solid lines represent difference spectra between 0.6 and 0 M urea.

turation curve for any of the three proteins. However, no significant changes were seen in the spectra between 0 and 1 M urea for either TCR. This minimal effect of urea on the TCRs is especially clear when examining difference spectra between data collected at 0.6 M urea, the highest concentration used in the binding and dissociation experiments, and 0

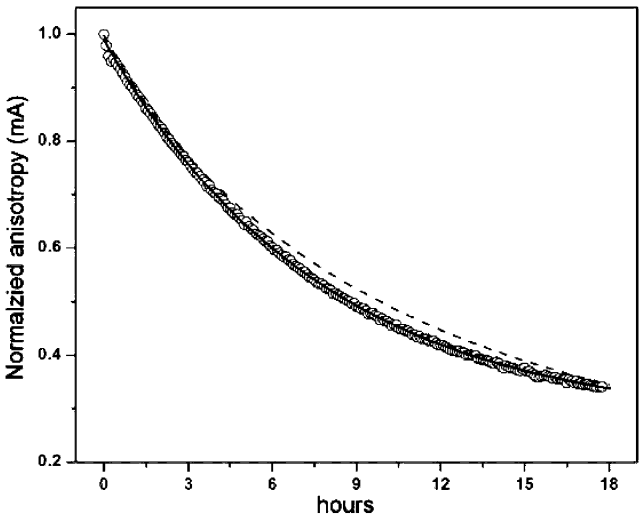

FIGURE 4: Urea (0.6 M) has only a marginal influence on dissociation of the Tax peptide from HLA-A2 as measured by steady-state fluorescence anisotropy. Circles show data collected in 0.6 M urea; the solid line is a fit to a single-exponential decay. The dashed line represents dissociation in 0 M urea from ref *19*.

M urea (solid lines in Figure 3A,B). As a second control for the effects of urea on receptor activity, we compared the activities (RU_{max}) of A6 and B7 SPR sensor surfaces measured in the absence of urea and in the presence of 0.6 M urea. These data indicated that 0.6 M urea resulted in modest and reversible reductions in activity of 8 ± 3% for the A6 surface and 8 ± 2% for the B7 surface (for comparison, experiments where the temperature was shifted from 12.5 to 28.5 °C resulted in activity reductions of 16 ± 2% for A6 and 30 ± 4% for B7; R. Davis-Harrison and B. M. Baker, unpublished results).

Urea had a larger effect on the Tax/HLA-A2 complex than the TCRs, as evident by the difference spectrum in Figure 3C. As significant destabilization of the molecule should result in faster peptide dissociation, we further examined the effects of urea on the Tax/HLA-A2 complex by measuring the rate of peptide dissociation using fluorescence anisotropy. In this experiment (Figure 4), 0.6 M urea reduced the half-life of the peptide−MHC complex from 7.6 to 5.3 h at 25 °C (amounting to a 30% increase in peptide off-rate). By comparison, a shift from 25 to 37 °C results in a much more substantial drop to 1.1 h (an 86% increase in peptide off-rate) (*19*). We concluded that although 0.6 M urea may have a small effect on the Tax/HLA-A2, it does not significantly destabilize the peptide/MHC complex (low concentrations of Tax/HLA-A2 were avoided and samples were stored at 4 °C prior to each injection to limit any influence from weaker peptide binding).

The Amount of Solvent-Accessible Surface Buried in the A6 and B7 Binding Transition States. Based on the TCR-Tax/HLA-A2 crystal structures, A6 and B7 bury ∼2000 Å^2 of solvent-accessible surface area in the bound state (*10*, *13*, *14*). The *m* value analysis thus yields an A6-Tax/HLA-A2 transition state that buries 1394 Å^2 and a B7-Tax/HLA-A2 transition state that buries 1306 Å^2. However, these calculations assume a rigid body interaction, which may not be the case for many TCR−ligand interactions (e.g., refs *36*−*38*). Although the structure of the unligated Tax/HLA-A2 molecule indicates only minor conformational differences between the bound and free states (*14*, *39*), the structures of the unligated A6 and B7 TCRs have not been determined. However, based on their fast binding kinetics relative to other TCR-peptide/MHC interactions, neither A6 nor B7 TCRs are predicted to populate significantly different conformational states prior to binding (*10*, *40*). In support of this prediction, Chen et al. recently showed that the structure of the 1G4 TCR, which binds the NY-$ESO_{157-165}$ peptide presented by HLA-A2 at a rate slightly slower than A6 or B7 TCRs bind Tax/HLA-A2, is very similar in both the bound and free states (*41*).

Table 2: Solvent-Accessible Surface Area (Å^2) Buried in the A6 and B7 TCR-Tax/HLA-A2 Complexes

	crystal structure[a]	MD max RMSD[b]	MD average[c]
	A6 Complex		
surface area buried in bound state	1991	2174	1482 ± 33
surface area buried in transition state ensemble[d]	1394 ± 100	1522 ± 109	1545 ± 106
	B7 Complex		
surface area buried in bound state	2009	2141	2117 ± 29
surface area buried in transition state ensemble[d]	1306 ± 141	1392 ± 150	1376 ± 148

[a] Calculated using coordinates from the A6- or B7-Tax/HLA-A2 crystal structures for the free TCRs and CDR loops. Assumes a rigid body interaction. [b] Calculated using the coordinates for the free TCRs from the MD simulations that showed the highest backbone RMSD relative to the crystal structures for the six CDR loops. See Supporting Information for more detail. [c] Calculated using the average solvent-accessible surface area of the free TCRs calculated over the length of the MD simulations, excluding the first 1 ns. Errors are the standard deviation of the mean. [d] Equal to total surface area buried multiplied by *m*-value ratio.

Nonetheless, even small conformational differences in the CDR loops between the free and bound states could impact the calculations of buried surface areas and influence our pictures of the two transition states. To address this, we performed unrestrained explicit-solvent molecular dynamics simulations of the free A6 and B7 TCRs. Using coordinates output every 2 fs, we recalculated the amount of surface area that would be buried by the A6 and B7 TCRs (additional details of the MD simulations are provided as Supporting Information). Table 2 lists the amount of surface area buried in the two transition states for three cases: (1) surface area buried calculated using the TCR conformations present in the two crystal structures, (2) surface area buried calculated using the TCR conformations from the MD simulations that show the greatest change in CDR loop conformation relative to the crystal structures, and (3) the average amount of surface buried calculated using each set of coordinates output from the MD simulations. Inclusion of the MD data increases the amount of surface area buried in each interaction, indicating that the MD simulations result in conformations with greater solvent accessibility. Using the simulated coordinates raises the solvent-accessible surface area buried in the transition states to ∼1500 Å^2 for A6 and ∼1400 Å^2 for B7.

The shifts seen in the MD simulations for the A6 TCRs are reflective of those observed experimentally in A6 recognition of variant Tax peptides presented by HLA-A2

Table 3: Kinetics, Affinities, and Φ Values for Wild-Type and Mutant A6 and B7 Recognition of Native and Position 5 Variants of the Tax Peptide[a]

peptide	TCR	K_D (μM)	k_{off} (s^{-1})	k_{on} (M^{-1} s^{-1})	$\Delta\Delta G°$ (kcal/mol)	$\Delta\Delta G^{‡}_{on}$ (kcal/mol)	Φ
native Tax	A6	2.23 ± 0.10	0.11	$4.90 \pm 0.02 \times 10^4$			
	B7	1.35 ± 0.04	0.13	$9.60 \pm 0.03 \times 10^4$			
Tax-Y5F	A6	2.79 ± 0.39	0.11	$4.0 \pm 0.1 \times 10^4$	0.13 ± 0.09	0.12 ± 0.28	0.91 ± 0.63
	B7	6.49 ± 0.17	0.42	$6.50 \pm 0.02 \times 10^4$	0.93 ± 0.02	0.23 ± 0.02	0.25 ± 0.02
Tax-Y5A	A6	33 ± 5	0.50	$1.2 \pm 0.3 \times 10^4$	1.60 ± 0.01	0.83 ± 0.15	0.52 ± 0.10
	B7	ND[b]	ND				ND
Tax-Y5W	A6	10 ± 1	0.30	$2.9 \pm 0.2 \times 10^4$	0.89 ± 0.06	0.31 ± 0.05	0.35 ± 0.05
	B7	35 ± 1	0.13	$3.7 \pm 0.1 \times 10^3$	1.93 ± 0.02	1.93 ± 0.02	1.00 ± 0.02
native Tax	A6 S31αA	5.48 ± 0.24	0.14	$2.5 \pm 0.1 \times 10^4$	0.53 ± 0.04	0.40 ± 0.03	0.74 ± 0.08
	B7 Y104βA	2.99 ± 0.10	0.13	$4.2 \pm 0.1 \times 10^4$	0.47 ± 0.03	0.49 ± 0.03	1.04 ± 0.08

[a] Values at 25 °C in HBS-EP buffer. Data for the native and Y5F peptides are from ref *10*, data for the Y5A peptide are from ref *43*, and data for the Y5W peptide and TCR mutants are from this work. [b] Insufficient binding was seen with B7 and the Y5A variant to determine binding affinities or kinetics.

(*21*, *42*) (see Supporting Information). The shifts include changes in CDR loop positions, including CDR3α and CDR3β (maximum shifts of 4.4 and 4.8 Å at the apex of the loops, respectively), but the loops are not wholly remodeled, as seen in the structures of A6 with the Tax-V7R variant (*21*) and the Tax-5K-IBA variant (*42*). They also include small shifts in α and β domain positioning, as also seen in the A6-Tax-5K-IBA/HLA-A2 structure (*42*). Although as indicated above there is no structure of the free A6 TCR which would be best for comparing with the results of the MD simulations, the observation that the simulations capture the kinds of structural changes seen with A6 supports their use here. Other than the structure with the Tax peptide, there are no additional structural data for the B7 TCR. However, the B7 MD simulations result in similar structural changes as seen in A6: shifts in CDR loop position (maximum of 6.7 Å for CDR3α and 5.0 Å for CDR3β) and small changes in domain orientation, which we anticipate mimic those observed experimentally with A6.

Participation of Tyr5 in the A6 and B7 Binding Transition States. The buried surface areas determined by *m*-value analysis do not indicate what structures are present at the transition states, nor do they indicate what intermolecular contacts may or may not be present. As opposed to *m* values, Φ analysis allows one to directly evaluate whether a given amino acid position participates in a transition state (*8*). Indeed, Φ analysis and *m* values are frequently used as complementary approaches to investigate the native-like character of protein folding transition states (e.g., refs *27*−*31*). For binding, a Φ value for an amino acid position is defined as $\Delta\Delta G^{‡}_{on}/\Delta\Delta G^{\circ}_{eq}$, where $\Delta\Delta G^{‡}_{on}$ represents the effect of a mutation on the height of the transition state barrier relative to the unbound state, and $\Delta\Delta G^{\circ}_{eq}$ represents the effect of a mutation on the overall binding free energy. A Φ value near 1 indicates that any destabilizing effects of a mutation arise only from a decrease in the on-rate and is interpreted to mean that any stabilizing interactions made to the site of mutation are fully formed in the binding transition state. A Φ value of zero indicates that any destabilizing effects of a mutation arise only from an increase in the off-rate and is interpreted to indicate that stabilizing interactions made to the mutated position are only formed as the transition state relaxes into the fully bound state. Intermediate Φ values are usually taken to indicate partial or weakened participation of the mutated position in the transition state.

We were particularly interested in the potential participation of peptide surface in the binding transition states. In the structures of both A6 and B7 with Tax/HLA-A2, Tyr5 of the Tax peptide projects up from the plane of the MHC α1/α2 helices into pockets formed by multiple CDR loops, including CDR3α and CDR3β, and in A6, CDR1α (*13*, *14*). Tyr5 is thus arguably the best position in the Tax/HLA-A2 molecule to evaluate the participation of peptide surface in the A6 and B7 binding transition states. Data for the A6 and B7 TCRs binding Tyr5 → Ala (Y5A) and Tyr5 → Phe (Y5F) variants of the Tax peptide presented by HLA-A2 are available (*10*, *43*). We also collected new data on the binding of A6 and B7 to the Tyr5 → Trp (Y5W) Tax variant. Binding affinities and kinetics as well as Φ values calculated from these data are shown in Table 3 (Biacore data for the Y5W variant are shown in the Supporting Information).

For the A6 TCR, the position 5 Φ values range from 0.91 to 0.35. Although the upper value of 0.9 for the Y5F substitution has a large error (±0.6, resulting from the very small $\Delta\Delta G°$), the values for the Y5A and Y5W substitutions are considerably more reliable (0.52 ± 0.10 and 0.35 ± 0.05). Altogether, the mean value for the A6 data is 0.6 (0.4 if the value of 0.9 is disregarded). For the B7 TCR, the position 5 Φ values range from 1.0 to 0.25, with a mean of 0.6 (data to calculate a Φ value for the B7 TCR with the Y5A substitution are unavailable due to a lack of detectable binding of B7 to the Tax Y5A variant; J. R. Clemens and B. M. Baker, unpublished results). These data, encompassing multiple substitutions at position 5, strongly suggest that stabilizing interactions to Tyr5 of the Tax peptide are formed in both the A6 and B7 binding transition states.

To further test whether Tyr5 participates in the A6 and B7 TCR binding transition states, we evaluated by Φ analysis select amino acids in A6 and B7 that contact Tyr5 in the TCR-Tax/HLA-A2 crystal structures. In A6, we chose Ser31 of CDR1α, whose side chain hydrogen bonds with the Tyr5 side chain hydroxyl at the top of the "Tyr5 pocket" in A6 (*14*). In B7, we chose Tyr104 of CDR3β, whose side chain contacts the aromatic ring of the Tyr5 side chain, forming one wall of the Tyr5 pocket in B7 (*13*). Other candidates were excluded as they either were very near the limit of our definition of an interatomic contact (distances ≤4 Å) or involved charged amino acids participating in long-range electrostatic interactions with HLA-A2 (*40*). Binding affinities, kinetics, and Φ values for the interaction of the A6

S31αA and B7 Y104β TCR mutants with native Tax/HLA-A2 are shown in Table 3 (Biacore data are shown in the Supporting Information). The Φ values, 0.74 ± 0.08 for position 31α in A6 and 1.04 ± 0.08 for position 104β in B7, further support the conclusion that stabilizing contacts to Tyr5 are formed within both TCR binding transition states. Moreover, together with the Φ for Tyr5, the data imply that the environment around Tyr5 in the two binding transition states is similar to that seen in the bound states.

Transition State Models Based on the Structures of the Bound States Require CDR3 Participation in the Binding Transition States. Although inconsistent with the two-step model (*9*), the *m* and Φ value experiments only give a limited picture of the nature of the A6 and B7 binding transition states: burial of a considerable amount of solvent-accessible surface area and bound-like contacts to and from Tyr5 of the Tax peptide. To date, most work on the nature of protein binding transition states has assumed that binding pathways follow a smooth energy funnel toward the bound state (*16*, *44*−*46*), with a low probability for contacts in the binding transition state that are not present in the bound state. This assumption follows from a considerable body of work in protein folding, in which theoretical folding models based only on the topology of the native state are able to accurately reproduce a wide range of structural, thermodynamic, and kinetic observations (recently reviewed in ref *17*), and builds on the landscape theory of protein folding (*47*), also applicable to binding (*48*, *49*). If we assume that this "principle of minimal frustration" (*15*) holds for the A6 and B7 interactions with Tax/HLA-A2, we can use the structures of the bound states to generate models of the A6 and B7 binding transition states.

Table 4 lists the amount of surface area buried by each CDR loop (and loop combinations) in the A6 and B7 complexes, using the crystallographic structures as well as the coordinates of the free TCRs generated by the MD simulations (to aid in interpretation of Table 4, images showing the position of each loop on Tax/HLA-A2 are available in the Supporting Information). For the A6 TCR, transition state models that are compatible with these data include those which bury significant portions of one or more of the α chain loops along with CDR3β or all of the α chain loops while the three β chain loops remain solvent exposed [using the X-ray coordinates, the A6 transition state buries 1394 ± 100 Å^2 (Table 2), CDR3β and CDR1α together bury 1368 Å^2, and all three α loops alone bury 1409 Å^2]. Despite the fact that the MD simulations indicate movement in the CDR loops (see Supporting Information), this motion does not greatly impact the solvent-accessible surface area buried by the various loops. We note that the Φ values exclude a model in which the requisite amount of surface area is buried by only CDR3α and CDR3β, as this would prevent the interaction between Tyr5 and Ser31 in CDR1α. Thus, while the surface area data do suggest that one or both CDR3 loops participate in the transition state, this does not seem to be at the expense of the germline-encoded loops.

Slightly different results are seen with the B7 TCR. Again assuming that the minimal frustration principle applies, through simple addition the amount of surface buried in the transition state *could* be achieved by burial of the four germline-encoded CDR loops [using the average MD coordinates, the transition state buries 1394 ± 100 Å^2 (Table 2), and the combined CDR1 and CDR2 loops bury 1388 Å^2 in the bound state]. Realistically, however, docking of all four germline-encoded loops could not occur without concomitant burial of at least some CDR3-associated surface. Furthermore, exclusion of CDR3β from the transition state would prevent the participation Tyr104β, in conflict with the Φ value data. Compatible transition state models for the B7 TCR thus include those which fully bury all three loops of the β chain and partially bury one or more loops of the α chain or, vice versa, those which fully bury all of the three α chain loops and partially bury one or more β chain loops. Other models within these two extremes are also possible, yet participation of CDR3β is mandatory.

Table 4: Solvent-Accessible Surface Area (Å^2) Buried by CDR Loops in the A6 and B7 TCR-Tax/HLA-A2 Complexes[a]

CDR loop or loop combination	crystal structure[b]	MD max RMSD[c]	MD average[d]
	A6 Complex		
α1	596	663	632 ± 10
α2	273	261	296 ± 8
α3	625	646	572 ± 21
α1 + α2	896	912	936 ± 13
α1 + α2 + α3	1409	1423	1398 ± 29
β1	72	103	91 ± 2
β2	14	53	51 ± 1
β3	772	811	800 ± 21
β1 + β2	86	144	126 ± 2
β1 + β2 + β3	813	870	870 ± 18
surface area buried in transition state[e]	1394 ± 100	1522 ± 109	1545 ± 106
	B7 Complex		
α1	660	673	690 ± 10
α2	324	413	343 ± 7
α3	560	550	595 ± 11
α1 + α2	927	989	933 ± 13
α1 + α2 + α3	1315	1513	1466 ± 21
β1	26	213	202 ± 3
β2	217	278	408 ± 4
β3	487	466	540 ± 12
β1 + β2	240	469	455 ± 6
β1 + β2 + β3	719	788	903 ± 15
surface area buried in transitions state[e]	1306 ± 141	1392 ± 150	1376 ± 148

[a] Surface area buried by CDR loops is total surface area, including contributions from the loops as well as the pMHC molecule. Values for loop combinations are not perfectly additive due to side-to-side packing of adjacent loops. [b] Calculated using coordinates from the A6- or B7-Tax/HLA-A2 crystal structures for the free TCRs and CDR loops. Assumes a rigid body interaction. [c] Calculated using the coordinates for the free TCRs from the MD simulations that showed the highest backbone RMSD relative to the crystal structures for the six CDR loops. See Supporting Information for more detail. [d] Calculated using the average solvent-accessible surface area of the free TCRs calculated over the length of the MD simulations, excluding the first 1 ns. Errors are the standard deviation of the mean. [e] From Table 2.

DISCUSSION

The role of the transition state in T cell receptor recognition of ligand has recently been highlighted by a two-step model in which TCR recognition proceeds via peptide-independent and peptide-dependent phases, demarcated at the binding transition state (*9*). The model neatly integrates TCR binding degeneracy with peptide specificity and has been implicated in a number of processes involving TCR recognition of ligand (*50*). Yet the model remains controversial (*50*, *51*), with data from different TCR−ligand

systems varying in their support of it (*9*, *12*, *52*, *53*). Here, we sought to characterize the binding transition states of A6 and B7, two αβ T cell receptors which recognize the Tax peptide presented by HLA-A2. Our goal was to provide additional experimental data relating to TCR binding transition states on which the two-step model could be tested or refined.

Using ratios of kinetic-to-equilibrium *m* values, we found that the two TCRs bury 65−70% of their total buried surface area in their binding transition states, a percentage comparable to that found in other protein−protein transition states (*32*−*34*). With the crystallographic structures of the TCR-peptide/MHC complexes as a reference, this amounts to burial of 1300−1400 Å^2 of solvent-accessible surface area. Attempting to account for conformational differences in the TCRs between the bound and unbound states increases the range to 1400−1500 Å^2. Either range reflects burial of a large amount of surface that would seem to necessitate a significant number of contacts made from the TCRs to the MHC-bound peptide (see Figure S1 in the Supporting Information). In support of this conclusion, Φ values for Tyr5 of the Tax peptide indicate that stabilizing contacts to this position are made in both the A6 and B7 binding transition states. Reciprocal Φ experiments with two positions in A6 and B7 that contact Tyr5 further support this conclusion and suggest that the environment around Tyr5 in the two transition states is similar to that seen in the two TCR-peptide/MHC crystal structures.

Additional insight into the nature of the two binding transition states was gained by considering the surface area buried by each CDR loop in the bound states. This analysis indicated that, for both A6 and B7, the amount of surface area buried in the two binding transition states requires participation of the CDR3 loops. The models generated from this analysis are speculative, as they require that contacts not present in the bound state are minimally populated along the binding pathway. Although generally accepted in studies of protein folding (*17*), the extent to which this principle of minimal frustration applies in binding reactions has not been experimentally well tested (*54*). However, these models are the simplest of those that are compatible with both the *m* and Φ value data. Alternative models for the binding transition states would require burial of a large amount of surface that is not buried in the bound state, with "non-native" contacts formed not just by Tyr5 but also Ser31α in A6 and Y104β in B7. Conceivably, this could arise from alternate CDR loop configurations within the transition states and a positioning of the TCRs on the MHC molecules in a fashion very different than seen in the crystal structures. To account for the data, however, the resulting transition states would need to be radically different from the bound states.

In the structure of the unligated Tax/HLA-A2 complex, Tyr5 of the peptide projects up from the center of the peptide backbone, which has a slight bulge characteristic of nonamers bound to class I MHC molecules. From the "side" of the Tax/HLA-A2 complex, if the β strands of the peptide binding groove are defined as the horizontal, the Tyr5 hydroxyl group defines a high point on the peptide/MHC, just above the extending side chains of Arg65 of the HLA-A2 α1 helix and Gln155 of the HLA-A2 α2 helix (see Supporting Information). Thus it is perhaps not too surprising that the A6 and B7 T cell receptors engage Tyr5 early in binding, as noted by Wu et al. in their derivation of the two-step model (*9*). However, projection of amino acid side chains above the MHC α1/α2 helices is not unusual in class I MHC complexes: a survey of class I peptide/MHC structures in the Protein Data Bank revealed a number of similar cases. Peptides presented in this fashion include nonamers, decamers, 11-mers, and in one case a 14-mer (*55*−*64*). Thus, although the exact details of any given TCR-peptide/MHC binding transition state are probably heavily dependent upon the nature of the bound peptide, contacts to projecting peptide side chains within TCR-peptide/MHC binding transition states may be relatively common.

It is striking that the transition states with A6 and B7 are so similar. In previous work, we have shown that A6 and B7 bind Tax/HLA-A2 with very different thermodynamics ($\Delta\Delta H°$ and $T\Delta\Delta S°$ are both near 10 kcal/mol at 25 °C), but this arises almost entirely from how the two receptors move from the transition state to the bound state ($\Delta\Delta H^{\ddagger}_{on}$ and $\Delta\Delta S^{\ddagger}_{on}$ are both near zero, with a negligible $\Delta\Delta C^{\ddagger}_{p,on}$) (*10*). Thus, not only do A6 and B7 bury very nearly the same amount of surface in their transition states, they bind with nearly identical activation thermodynamics. This could be indicative of very similar structures formed within the two transition states, an interpretation compatible with the *m* value and Φ value data presented here. Yet, A6 and B7 have different Vα domains, and their CDR3 loops are entirely different. In the face of these sequence differences, how could the activation thermodynamics and the nature of the two transition states be so similar? Perhaps the A6 and B7 transition states consist of actual intermolecular *contacts* to protruding side chains only (such as Tyr5), with the majority of the association energetics and surface removed from bulk water, resulting not from intermolecular *contacts* but from dehydration of similar surfaces as the molecules approach, as discussed by Gabdoulline and Wade in their analysis of protein−protein encounter complexes (*65*). This binding model would limit the formation of different interatomic contacts that could give rise to differing activation energies, yet is still compatible with the *m* and Φ value data indicating removal of a significant amount of surface from bulk solvent and a bound-like environment around Tyr5 of the Tax peptide.

The results with A6 and B7 are reminiscent of the recent work of Lee et al., who studied the binding of the G10 TCR to an HIV epitope and a single amino acid variant presented by HLA-A2 (*12*). Remarkably, the TCR bound both peptide/MHC complexes with the same activation thermodynamics, despite the fact that the peptides were found to occupy different conformations in the free peptide/MHC complexes. Assuming the peptides adopted the same conformation in the TCR-bound state, the authors interpreted their results as the TCR initially engaging the MHC molecule relatively independent of the peptide and then contacting the peptide as the transition state decayed to the bound state, i.e., in the context of the two-step model. However, it is also possible that the G10 TCR initially engages these ligands in a fashion similar to that noted above (minimal interatomic contacts along with the exclusion of bulk solvent, followed by formation of specific contacts as the transition state decays). Additional work is needed to distinguish between these possibilities.

If the two-step model as originally formulated is not generally applicable, is there an alternative which might permit a physical distinction between the peptide and the MHC molecule in TCR recognition of ligand? Perhaps certain TCR binding reactions proceed via the formation of a binding *intermediate* resulting from strong interactions with the MHC molecule [i.e., a state whose free energy is in between fully bound and free, with fully bound and free separated by multiple transition state barriers, as seen in the interaction between RNase S and the S-peptide (*32*)]. Although thus far there are no physical data suggesting the existence of such an intermediate in TCR binding reactions, its presence would be expected to be strongly dependent on the nature of individual TCRs and peptides, and it could be selected against during TCR positive selection (*66*). Detection of such an intermediate would therefore require careful selection of systems and likely kinetic methods without the low temporal resolution of surface plasmon resonance (*67*).

ACKNOWLEDGMENT

We thank Samy Meroueh and Alison Wojnarowicz for expert assistance, John R. Clemens for providing unpublished binding data, and Jim Horn for helpful discussion.

SUPPORTING INFORMATION AVAILABLE

Data as described in the text. This material is available free of charge via the Internet at http://pubs.acs.org.

REFERENCES

1. Rudolph, M. G., Luz, J. G., and Wilson, I. A. (2002) Structural and thermodynamic correlates of T cell signaling, *Annu. Rev. Biophys. Biomol. Struct. 31*, 121−149.
2. Wucherpfennig, K. W. (2004) T cell receptor crossreactivity as a general property of T cell recognition, *Mol. Immunol. 40*, 1009−1017.
3. Shih, F. F., and Allen, P. M. (2004) T cells are not as degenerate as you think, once you get to know them, *Mol. Immunol. 40*, 1041−1046.
4. Maynard, J., Petersson, K., Wilson, D. H., Adams, E. J., Blondelle, S. E., Boulanger, M. J., Wilson, D. B., and Garcia, K. C. (2005) Structure of an autoimmune T cell receptor complexed with class II peptide-MHC: insights into MHC bias and antigen specificity, *Immunity 22*, 81−92.
5. Zerrahn, J., Held, W., and Raulet, D. H. (1997) The MHC reactivity of the T cell repertoire prior to positive and negative selection, *Cell 88*, 627−636.
6. Boniface, J. J., Reich, Z., Lyons, D. S., and Davis, M. M. (1999) Thermodynamics of T cell receptor binding to peptide-MHC: evidence for a general mechanism of molecular scanning, *Proc. Natl. Acad. Sci. U.S.A. 96*, 11446−11451.
7. Krogsgaard, M., Li, Q. J., Sumen, C., Huppa, J. B., Huse, M., and Davis, M. M. (2005) Agonist/endogenous peptide-MHC heterodimers drive T cell activation and sensitivity, *Nature 434*, 238−243.
8. Fersht, A. R. (1995) Characterizing transition states in protein folding: an essential step in the puzzle, *Curr. Opin. Struct. Biol. 5*, 79−84.
9. Wu, L. C., Tuot, D. S., Lyons, D. S., Garcia, K. C., and Davis, M. M. (2002) Two-step binding mechanism for T-cell receptor recognition of peptide MHC, *Nature 418*, 552−556.
10. Davis-Harrison, R. L., Armstrong, K. M., and Baker, B. M. (2005) Two different T cell receptors use different thermodynamic strategies to recognize the same peptide/MHC ligand, *J. Mol. Biol. 346*, 533−550.
11. Anikeeva, N., Lebedeva, T., Krogsgaard, M., Tetin, S. Y., Martinez-Hackert, E., Kalams, S. A., Davis, M. M., and Sykulev, Y. (2003) Distinct molecular mechanisms account for the specificity of two different T-cell receptors, *Biochemistry 42*, 4709−4716.
12. Lee, J. K., Stewart-Jones, G., Dong, T., Harlos, K., Di, Gleria, K., Dorrell, L., Douek, D. C., van der Merwe, P. A., Jones, E. Y., and McMichael, A. J. (2004) T cell cross-reactivity and conformational changes during TCR engagement, *J. Exp. Med. 200*, 1455−1466.
13. Ding, Y. H., Smith, K. J., Garboczi, D. N., Utz, U., Biddison, W. E., and Wiley, D. C. (1998) Two human T cell receptors bind in a similar diagonal mode to the HLA-A2/Tax peptide complex using different TCR amino acids, *Immunity 8*, 403−411.
14. Garboczi, D. N., Ghosh, P., Utz, U., Fan, Q. R., Biddison, W. E., and Wiley, D. C. (1996) Structure of the complex between human T-cell receptor, viral peptide and HLA-A2, *Nature 384*, 134−141.
15. Bryngelson, J. D., and Wolynes, P. G. (1987) Spin glasses and the statistical mechanics of protein folding, *Proc. Natl. Acad. Sci. U.S.A. 84*, 7524−7528.
16. Levy, Y., Cho, S. S., Onuchic, J. N., and Wolynes, P. G. (2005) A survey of flexible protein binding mechanisms and their transition states using native topology based energy landscapes, *J. Mol. Biol. 346*, 1121−1145.
17. Baker, D. (2000) A surprising simplicity to protein folding, *Nature 405*, 39−42.
18. Myszka, D. G. (1999) Improving biosensor analysis, *J. Mol. Recognit. 12*, 279−284.
19. Binz, A. K., Rodriguez, R. C., Biddison, W. E., and Baker, B. M. (2003) Thermodynamic and kinetic analysis of a peptide-class I MHC interaction highlights the noncovalent nature and conformational dynamics of the class I heterotrimer, *Biochemistry 42*, 4954−4961.
20. Rodriguez, R., Chinea, G., Lopez, N., Pons, T., and Vriend, G. (1998) Homology modeling, model and software evaluation: three related resources, *Bioinformatics 14*, 523−528.
21. Ding, Y. H., Baker, B. M., Garboczi, D. N., Biddison, W. E., and Wiley, D. C. (1999) Four A6-TCR/peptide/HLA-A2 structures that generate very different T cell signals are nearly identical, *Immunity 11*, 45−56.
22. Case, D. A., Darden, T. A., Cheatham, T. E., Simmerling, C. L., Wang, J., Duke, R. E., Luo, R., Merz, K. M., Wang, B., Pearlman, D. A., Crowley, M., Brozell, S., Tsui, V., Gohlke, H., Mongan, J., Hornak, V., Cui, G., Beroza, P., Schafmeister, C., Caldwell, J. W., Ross, W. S., and Kollman, P. A. (2004) AMBER 8, University of California, San Francisco.
23. Zarrine-Afsar, A., and Davidson, A. R. (2004) The analysis of protein folding kinetic data produced in protein engineering experiments, *Methods 34*, 41−50.
24. Zou, Q., Habermann-Rottinghaus, S. M., and Murphy, K. P. (1998) Urea effects on protein stability: Hydrogen bonding and the hydrophobic effect, *Proteins:Struct., Funct., Genet. 31*, 107−115.
25. Makhatadze, G. I., and Privalov, P. L. (1992) Protein interactions with urea and guanidinium chloride. A calorimetric study, *J. Mol. Biol. 226*, 491−505.
26. Myers, J. K., Pace, C. N., and Scholtz, J. M. (1995) Denaturant m values and heat capacity changes: Relation to changes in accessible surface areas of protein unfolding, *Protein Sci. 4*, 2138−2148.
27. Sanchez, I. E., and Kiefhaber, T. (2003) Hammond behavior versus ground state effects in protein folding: evidence for narrow free energy barriers and residual structure in unfolded states, *J. Mol. Biol. 327*, 867−884.
28. Fowler, S. B., and Clarke, J. (2001) Mapping the folding pathway of an immunoglobulin domain: structural detail from phi value analysis and movement of the transition state, *Structure 9*, 355−366.
29. Parker, M. J., Spencer, J., and Clarke, A. R. (1995) An integrated kinetic analysis of intermediates and transition states in protein folding reactions, *J. Mol. Biol. 253*, 771−786.
30. Matthews, J. M., and Fersht, A. R. (1995) Exploring the energy surface of protein-folding by structure-reactivity relationships and engineered proteins—observation of Hammond behavior for the gross structure of the transition-state and anti-Hammond behavior for structural elements for unfolding folding of barnase, *Biochemistry 34*, 6805−6814.
31. Itzhaki, L. S., Otzen, D. E., and Fersht, A. R. (1995) The structure of the transition state for folding of chymotrypsin inhibitor 2 analysed by protein engineering methods: evidence for a nucleation-condensation mechanism for protein folding, *J. Mol. Biol. 254*, 260−288.

32. Goldberg, J. M., and Baldwin, R. L. (1998) Kinetic mechanism of a partial folding reaction. 1. Properties of the reaction and effects of denaturants, *Biochemistry 37*, 2546−2555.
33. Gloss, L. M., and Matthews, C. R. (1998) Mechanism of folding of the dimeric core domain of *Escherichia coli* Trp repressor: A nearly diffusion-limited reaction leads to the formation of an on-pathway dimeric intermediate, *Biochemistry 37*, 15990−15999.
34. Dwyer, J. J., Dwyer, M. A., and Kossiakoff, A. A. (2001) High affinity RNase S-peptide variants obtained by phage display have a novel "hot-spot" of binding energy, *Biochemistry 40*, 13491−13500.
35. Baker, B. M., and Wiley, D. C. (2001) alpha beta T cell receptor ligand-specific oligomerization revisited, *Immunity 14*, 681−692.
36. Reiser, J. B., Gregoire, C., Darnault, C., Mosser, T., Guimezanes, A., Schmitt-Verhulst, A. M., Fontecilla-Camps, J. C., Mazza, G., Malissen, B., and Housset, D. (2002) A T cell receptor CDR3beta loop undergoes conformational changes of unprecedented magnitude upon binding to a peptide/MHC class I complex, *Immunity 16*, 345−354.
37. Kjer-Nielsen, L., Clements, C. S., Purcell, A. W., Brooks, A. G., Whisstock, J. C., Burrows, S. R., McCluskey, J., and Rossjohn, J. (2003) A structural basis for the selection of dominant alphabeta T cell receptors in antiviral immunity, *Immunity 18*, 53−64.
38. Garcia, K. C., Degano, M., Pease, L. R., Huang, M., Peterson, P. A., Teyton, L., and Wilson, I. A. (1998) Structural basis of plasticity in T cell receptor recognition of a self peptide-MHC antigen, *Science 279*, 1166−1172.
39. Madden, D. R., Garboczi, D. N., and Wiley, D. C. (1993) The antigenic identity of peptide-MHC complexes: a comparison of the conformations of five viral peptides presented by HLA-A2, *Cell 75*, 693−708 [erratum: (1994) *Cell 76*, 410].
40. Gagnon, S. J., Borbulevych, O. Y., Davis-Harrison, R. L., Baxter, T. K., Clemens, J. R., Armstrong, K. M., Turner, R. V., Damirjian, M., Biddison, W. E., and Baker, B. M. (2005) Unraveling a hotspot for TCR recognition on HLA-A2: evidence against the existence of peptide-independent TCR binding determinants, *J. Mol. Biol. 353*, 556.
41. Chen, J.-L., Stewart-Jones, G., Bossi, G., Lissin, N. M., Wooldridge, L., Choi, E. M. L., Held, G., Dunbar, P. R., Esnouf, R. M., Sami, M., Boulter, J. M., Rizkallah, P., Renner, C., Sewell, A., van der Merwe, P. A., Jakobsen, B. K., Griffiths, G., Jones, E. Y., and Cerundolo, V. (2005) Structural and kinetic basis for heightened immunogenicity of T cell vaccines, *J. Exp. Med. 201*, 1243−1255.
42. Gagnon, S. J., Borbulevych, O. Y., Davis-Harrison, R. L., Turner, R. V., Damirjian, M., Wojnarowicz, A., Biddison, W. E., and Baker, B. M. (2006) T cell receptor recognition via cooperative conformational plasticity, *J. Mol. Biol. 363*, 228−243.
43. Baker, B. M., Ding, Y. H., Garboczi, D. N., Biddison, W. E., and Wiley, D. C. (2000) Structural, biochemical, and biophysical studies of HLA-A2/altered peptide ligands binding to viral-peptide-specific human T-cell receptors, *Cold Spring Harbor Symp. Quant. Biol. 64*, 235−241.
44. Levy, Y., Wolynes, P. G., and Onuchic, J. N. (2004) Protein topology determines binding mechanism, *Proc. Natl. Acad. Sci. U.S.A. 101*, 511−516.
45. Yang, S., Cho, S. S., Levy, Y., Cheung, M. S., Levine, H., Wolynes, P. G., and Onuchic, J. N. (2004) From the cover: domain swapping is a consequence of minimal frustration, *Proc. Natl. Acad. Sci. U.S.A. 101*, 13786−13791.
46. Tovchigrechko, A., and Vakser, I. A. (2001) How common is the funnel-like energy landscape in protein-protein interactions?, *Protein Sci. 10*, 1572−1583.
47. Dill, K. A., and Chan, H. S. (1997) From Levinthal to pathways to funnels, *Nat. Struct. Biol. 4*, 10−19.
48. Miller, D. W., and Dill, K. A. (1997) Ligand binding to proteins: The binding landscape model, *Protein Sci. 6*, 2166−2179.
49. Ma, B., Kumar, S., Tsai, C.-J., and Nussinov, R. (1999) Folding funnels and binding mechanisms, *Protein Eng. 12*, 713−720.
50. Krogsgaard, M., and Davis, M. M. (2005) How T cells "see" antigen, *Nat. Immunol. 6*, 239−245.
51. Housset, D., and Malissen, B. (2003) What do TCR-pMHC crystal structures teach us about MHC restriction and alloreactivity?, *Trends Immunol. 24*, 429−437.
52. Reiser, J. B., Darnault, C., Gregoire, C., Mosser, T., Mazza, G., Kearney, A., van der Merwe, P. A., Fontecilla-Camps, J. C., Housset, D., and Malissen, B. (2003) CDR3 loop flexibility contributes to the degeneracy of TCR recognition, *Nat. Immunol. 4*, 241−247.
53. Borg, N. A., Ely, L. K., Beddoe, T., Macdonald, W. A., Reid, H. H., Clements, C. S., Purcell, A. W., Kjer-Nielsen, L., Miles, J. J., Burrows, S. R., McCluskey, J., and Rossjohn, J. (2005) The CDR3 regions of an immunodominant T cell receptor dictate the "energetic landscape" of peptide-MHC recognition, *Nat. Immunol. 6*, 171−180.
54. Levy, Y., and Onuchic, J. N. (2006) Mechanisms of protein assembly: lessons from minimalist models, *Acc. Chem. Res. 39*, 135−142.
55. Miles, J. J., Elhassen, D., Borg, N. A., Silins, S. L., Tynan, F. E., Burrows, J. M., Purcell, A. W., Kjer-Nielsen, L., Rossjohn, J., Burrows, S. R., and McCluskey, J. (2005) CTL recognition of a bulged viral peptide involves biased TCR selection, *J. Immunol. 175*, 3826−3834.
56. Stewart-Jones, G. B., di Gleria, K., Kollnberger, S., McMichael, A. J., Jones, E. Y., and Bowness, P. (2005) Crystal structures and KIR3DL1 recognition of three immunodominant viral peptides complexed to HLA-B*2705, *Eur. J. Immunol. 35*, 341−351.
57. Meijers, R., Lai, C. C., Yang, Y., Liu, J. H., Zhong, W., Wang, J. H., and Reinherz, E. L. (2005) Crystal structures of murine MHC Class I H-2 D(b) and K(b) molecules in complex with CTL epitopes from influenza A virus: implications for TCR repertoire selection and immunodominance, *J. Mol. Biol.* 345, 1099−110.
58. Stewart-Jones, G. B., Gillespie, G., Overton, I. M., Kaul, R., Roche, P., McMichael, A. J., Rowland-Jones, S., and Jones, E. Y. (2005) Structures of three HIV-1 HLA-B*5703-peptide complexes and identification of related HLAs potentially associated with long-term nonprogression, *J. Immunol. 175*, 2459−2468.
59. Gillespie, G. M. A., Stewart-Jones, G., Rengasamy, J., Beattie, T., Bwayo, J. J., Plummer, F. A., Kaul, R., McMichael, A. J., Easterbrook, P., Dong, T., Jones, E. Y., and Rowland-Jones, S. L. (2006) Strong TCR conservation and altered T cell cross-reactivity characterize a B*57-restricted immune response in HIV-1 infection, *J. Immunol 177*, 3893−3902.
60. Macdonald, W. A., Purcell, A. W., Mifsud, N. A., Ely, L. K., Williams, D. S., Chang, L., Gorman, J. J., Clements, C. S., Kjer-Nielsen, L., Koelle, D. M., Burrows, S. R., Tait, B. D., Holdsworth, R., Brooks, A. G., Lovrecz, G. O., Lu, L., Rossjohn, J., and McCluskey, J. (2003) A naturally selected dimorphism within the HLA-B44 supertype alters class I structure, peptide repertoire, and T cell recognition, *J. Exp. Med. 198*, 679−691.
61. Zernich, D., Purcell, A. W., Macdonald, W. A., Kjer-Nielsen, L., Ely, L. K., Laham, N., Crockford, T., Mifsud, N. A., Bharadwaj, M., Chang, L., Tait, B. D., Holdsworth, R., Brooks, A. G., Bottomley, S. P., Beddoe, T., Peh, C. A., Rossjohn, J., and McCluskey, J. (2004) Natural HLA class I polymorphism controls the pathway of antigen presentation and susceptibility to viral evasion, *J. Exp. Med. 200*, 13−24.
62. Cole, D. K., Pierre, J. R. F. G., Neil, I. W., Jonathan, M. B., John, I. B. M. S., George, F. G., and Bent, K. J. (2006) Crystal structure of HLA-A*2402 complexed with a telomerase peptide, *Eur. J. Immunol. 36*, 170−179.
63. Hulsmeyer, M., Fiorillo, M. T., Bettosini, F., Sorrentino, R., Saenger, W., Ziegler, A., and Uchanska-Ziegler, B. (2004) Dual, HLA-B27 subtype-dependent conformation of a self-peptide, *J. Exp. Med. 199*, 271−281.
64. Probst-Kepper, M., Hecht, H.-J., Herrmann, H., Janke, V., Ocklenburg, F., Klempnauer, J., van den Eynde, B. J., and Weiss, S. (2004) Conformational restraints and flexibility of 14-meric peptides in complex with HLA-B*3501, *J. Immunol. 173*, 5610−5616.
65. Gabdoulline, R. R., and Wade, R. C. (1999) On the protein-protein diffusional encounter complex, *J. Mol. Recognit. 12*, 226−234.
66. Ignatowicz, L., Kappler, J., and Marrack, P. (1996) The repertoire of T cells shaped by a single MHC/peptide ligand, *Cell 84*, 521−529.
67. Gakamsky, D. M., Luescher, I. F., and Pecht, I. (2004) T cell receptor-ligand interactions: A conformational preequilibrium or an induced fit, *Proc. Natl. Acad. Sci. U.S.A. 101*, 9063−9066.

BI061702P